scientific reports

Check for updates

OPEN

Whole genome DNA and RNA sequencing of whole blood elucidates the genetic architecture of gene expression underlying a wide range of diseases

Chunyu Liu[1,2,8]✉, Roby Joehanes[3,8]✉, Jiantao Ma[4], Yuxuan Wang[1], Xianbang Sun[1], Amena Keshawarz[3], Meera Sooda[3], Tianxiao Huan[3], Shih-Jen Hwang[3], Helena Bui[3], Brandon Tejada[3], Peter J. Munson[3], Cumhur Y. Demirkale[5], Nancy L. Heard-Costa[2,6], Achilleas N. Pitsillides[1], Gina M. Peloso[1], Michael Feolo[7], Nataliya Sharopova[7], Ramachandran S. Vasan[2,6] & Daniel Levy[2,3,8]✉

To create a scientific resource of expression quantitative trail loci (eQTL), we conducted a genome-wide association study (GWAS) using genotypes obtained from whole genome sequencing (WGS) of DNA and gene expression levels from RNA sequencing (RNA-seq) of whole blood in 2622 participants in Framingham Heart Study. We identified 6,778,286 *cis*-eQTL variant-gene transcript (eGene) pairs at $p < 5 \times 10^{-8}$ (2,855,111 unique *cis*-eQTL variants and 15,982 unique eGenes) and 1,469,754 *trans*-eQTL variant-eGene pairs at $p < 1e{-}12$ (526,056 unique *trans*-eQTL variants and 7233 unique eGenes). In addition, 442,379 *cis*-eQTL variants were associated with expression of 1518 long non-protein coding RNAs (lncRNAs). Gene Ontology (GO) analyses revealed that the top GO terms for *cis*-eGenes are enriched for immune functions (FDR < 0.05). The *cis*-eQTL variants are enriched for SNPs reported to be associated with 815 traits in prior GWAS, including cardiovascular disease risk factors. As proof of concept, we used this eQTL resource in conjunction with genetic variants from public GWAS databases in causal inference testing (e.g., COVID-19 severity). After Bonferroni correction, Mendelian randomization analyses identified putative causal associations of 60 eGenes with systolic blood pressure, 13 genes with coronary artery disease, and seven genes with COVID-19 severity. This study created a comprehensive eQTL resource via BioData Catalyst that will be made available to the scientific community. This will advance understanding of the genetic architecture of gene expression underlying a wide range of diseases.

Over the past decade, genome-wide association studies (GWAS) have revolutionized understanding of the genetic architecture of complex traits[1]. To date, GWAS have reported more than 59,000 associations (at $p < 5 \times 10^{-8}$) between common genetic variants and numerous phenotypes (GWAS Catalog, v1.0.2)[2]. Yet, despite the clear success of GWAS, most single-nucleotide polymorphisms (SNPs) identified in GWAS reside in non-coding regions[3–5] and do not illuminate causal mechanisms underlying SNP-trait associations[5]. We posit that many of these trait-associated non-coding SNPs are likely to be involved in the regulation of gene expression.

[1]Department of Biostatistics, School of Public Health, Boston University, Boston, MA, USA. [2]Framingham Heart Study, Framingham, MA, USA. [3]Population Sciences Branch, Division of Intramural Research, National Heart, Lung, and Blood Institute, National Institutes of Health, Bethesda, MD, USA. [4]Nutrition Epidemiology and Data Science, Friedman School of Nutrition Science and Policy, Tufts University, Boston, MA, USA. [5]Critical Care Medicine Department, Clinical Center, National Institutes of Health, Bethesda, MD, USA. [6]Departments of Medicine and Epidemiology, Boston University Schools of Medicine and Public Health, Boston, MA, USA. [7]National Center for Biotechnology Information, National Library of Medicine, National Institutes of Health, Bethesda, MD, USA. [8]These authors contributed equally: Chunyu Liu, Roby Joehanes and Daniel Levy. ✉email: liuc@bu.edu; roby.joehanes@nih.gov; levyd@nih.gov

Expression quantitative trait locus (eQTL) analysis seeks to identify genetic variants that affect the expression of local (*cis*) or distant (*trans*) genes (eGenes). Until recently, eQTL analysis has relied on high throughput microarray technologies and spawned a wave of genome-wide eQTL studies[6–11] including a recent study from our group[12]. These studies aided the understanding of the functional relevance of many GWAS results. Importantly, a hypothesis-free genome-wide eQTL approach permits the identification of new putatively functional loci without requiring previous knowledge of specific regulatory regions.

Most previous eQTL analyses were limited by small sample sizes and by the imprecision of microarrays. Newer technologies of RNA sequencing (RNA-seq) and whole genome sequencing (WGS) of DNA add greater precision and relevance to eQTL analyses. In conjunction with the National Heart, Lung, and Blood Institute's (NHLBI) Trans-Omics for Precision Medicine (TOPMed) Program[13], the Framingham Heart Study (FHS) has obtained whole genome sequencing (WGS) in ~ 6100 study participants to help understand the molecular basis of heart, lung, blood, and sleep disorders and to advance precision medicine. Among FHS participants with WGS, RNA-seq was obtained in 2622 participants. We conducted genome-wide eQTL analyses using high-precision genotypes obtained via WGS and gene expression levels from RNA-seq of whole blood. The primary objectives of this study were three-fold. Firstly, it sought to provide a scientific resource of *cis* and *trans* gene-level eQTL data to facilitate understanding of the genetic architecture of gene expression traits. Secondly, it was aimed to provide eQTL data for long noncoding RNAs (lncRNAs) that were not captured in prior array-based eQTL studies. Thirdly, it attempted to demonstrate the utility of the eQTL resource in causal inference analyses.

Results

Of the 2622 FHS participants in eQTL analyses, 720 participants were from the FHS Offspring cohort (mean age 71 ± 8 years; 59% women) and 1902 were from the Third Generation cohort (mean age 47 ± 8 years; 52% women) (Supplemental Table 1). We used 19,624,299 SNPs with a minor allele count (MAC) ≥ 10 and 58,870 expression levels in association analyses to identify gene-level eQTLs. We evaluated the genomic inflation factor (λ_{GC}). The observed $\lambda_{GC} = 1.03$, indicating that inflation was unlikely for the eQTL analyses (Supplemental Fig. 1).

Gene-level eQTL results. *cis-eQTLs.* *Cis*-eQTLs was defined as SNPs within 1 Mb of the transcription start sites (TSSs) of targeting genes. We identified 6,778,286 significant *cis*-eQTL variant-eGene pairs from 2,855,111 unique *cis*-eQTL variants and 15,982 unique eGenes (at $p < 5 \times 10^{-8}$) (Supplemental Table 2). The median number of *cis*-eQTL variants per gene was 183 (interquartile range = 47,463). The eGenes harboring the largest numbers of *cis*-eQTL variants are located in the human leukocyte antigen (*HLA*) or major histocompatibility complex (MHC) on chromosome 6, reflecting a large number of SNPs in strong linkage disequilibrium (LD) at the MHC locus[14]. Owing to the computational burden, we selected the strongest *cis*-eQTL variant (i.e., the lead variant) as that which had the lowest *p*-value per eGene. If several *cis*-eQTLs displayed the same *p*-value (i.e., they are in perfect LD, $r^2 = 1$), we randomly select one lead eQTL variant per eGene (Supplemental Table 3) and the top 25 pairs was displayed in Table 1. Of the 15,982 significant unique *cis*-eQTL variant-eGene pairs, 82.8% (n = 13,236) of SNPs were within 100 kb of the transcription start sites (TSSs) of the respective eGenes, 9.3% (n = 1486) within 101 kb–200 kb region, 5.7% (n = 909) within 201 kb–500 kb region, and 2.2% (n = 351) within 501 kb–1 Mb (Fig. 1A). Published GWAS and QTL analyses revealed that rare variants have larger effect sizes than common variants[6,15]. Therefore, we compared the median, 25th percentile, and 75th percentile of the absolute values of effect sizes for lead *cis*-eQTL variants across four variant groups based on minor allele frequencies (MAFs). We found that rare cis-eQTL variants displayed larger effect sizes (median effect size 0.44 versus 1.77 for *cis*-QTL variants with MAF in 0.1–0.5 versus *cis*-QTL variants with MAF in 0.003–0.01) (trend test $P < 0.001$) (Table 2).

trans-eQTLs. *Trans*-eQTLs referred to the SNPs that were beyond of 1 Mb of the TSSs of the eGenes on the same chromosome or those on the different chromosomes of the eGenes. We identified 1,469,754 significant *trans*-eQTL variant-eGene pairs ($p < 1e{-}12$) from 526,056 unique *trans*-eQTL variants and 7233 *trans*-eGenes (Table 3, Supplemental Table 4). The median number of significant-eQTL variants per eGene was 11 (interquartile range = 2, 76)[14]. With the same method used to select the lead *cis*-eQTL variants, we selected the lead trans-eQTL variant based on *p*-values for each *trans*-eGene, yielding 7233 unique *trans*-eQTL-eGene pairs (Supplemental Table 4). We further compared the effect sizes of the lead *trans*-eQTL variants based on their MAF. We found that rare *trans*-eQTL variants (MAF in 0.003–0.01) displayed larger effect sizes (median effect size 0.42 versus 2.38 for common *trans*-QTL variants (MAF in 0.1–0.5) (trend test $P < 0.001$) (Table 2).

Long noncoding RNA (lncRNA) eQTLs. lncRNAs are usually more than 200 bases in length, share no conserved sequence homology, and have variable functions[16]. Of the 58,870 transcripts captured by RNA-seq, 7696 (13%) are lncRNAs. Of the significant *cis*-eQTL variant-eGene pairs (n = 6,778,286, $p < 5e{-}8$), 565, 769 *cis*-eQTL variants are associated with expression of 1516 unique *cis*-lncRNAs (Supplemental Table 5). Of the significant *trans*-eQTL variant-eGene pairs ($p < 1e{-}12$), 164,386 *trans*-eQTL variants were associated with expression of 475 *trans*-lncRNAs (Supplemental Table 6). Three *cis*-eQTL-lncRNA pairs were observed among the top 25 *cis*-eQTL results (Table 1). The top *cis*-lncRNA, the MAP3K2 divergent transcript (MAP3K2-DT), is the only lncRNA that is located adjacent to a protein coding gene, the 5'-end of mitogen-activated protein kinase kinase kinase 2 (MAP3K2) on chromosome 2 (q14.3) (Supplemental Fig. 2). The correlation of expression of MAP3K2 and MAP3K2-DT was weak (Pearson correlation = 0.08; $p = 0.12$). Among the top 25 *trans*-eQTL pairs, we identified one *trans*-eQTL-lncRNA pair (Table 3). The top *trans*-lncRNA, AP001005.3 on chromosome 18, is not adjacent to any known genes.

Gene Symbol	SNP	Chr	SNP position	Gene start position	R^2	Beta	log10P	OA	EA	EAF	Type
PPIE	rs7513045	1	39,738,494	39,692,182	0.84	11.40	− 1029.25	G	T	0.36	protein_coding
CCDC163	rs4660860	1	45,480,561	45,493,866	0.90	− 3.10	− 1286.89	T	A	0.30	protein_coding
CYP26B1	rs13430651	2	72,215,195	72,129,238	0.81	1.98	− 920.005	G	A	0.15	protein_coding
MAP3K2-DT	rs2276683	2	127,389,186	127,389,130	0.88	− 1.61	− 1176.37	G	C	0.23	lincRNA
SLC12A7	rs35188965	5	1,104,823	1,050,384	0.81	− 29.87	− 915.459	C	T	0.44	protein_coding
ENC1	rs112772452	5	74,631,048	74,627,406	0.83	14.53	− 986.798	CA	C	0.11	protein_coding
ERAP2	rs2910686	5	96,916,885	96,875,939	0.85	36.98	− 1044.91	T	C	0.43	protein_coding
BTNL3	rs72494581	5	181,003,797	180,988,845	0.82	13.52	− 950.405	T	C	0.30	protein_coding
HLA-DRB5	rs68176300	6	32,558,713	32,517,353	0.83	− 178.13	− 1003.76	T	G	0.15	protein_coding
AL512625.3	rs1845054	9	62,906,092	62,856,999	0.83	− 1.19	− 993.655	T	C	0.13	lincRNA
CUTALP	rs13299616	9	120,832,525	120,824,828	0.86	− 23.25	− 1092.88	T	C	0.40	transcribed_unitary_pseudogene
LDHC	rs201993031	11	18,412,985	18,412,318	0.82	0.16	− 946.833	CCCTTCCTT	C	0.12	protein_coding
ACCS	rs2074038	11	44,066,439	44,065,925	0.83	16.69	− 997.26	G	T	0.11	protein_coding
FADS2	rs968567	11	61,828,092	61,792,980	0.88	31.41	− 1186.37	C	T	0.17	protein_coding
XRRA1	rs10899051	11	74,931,506	74,807,739	0.91	5.38	− 1327.88	G	A	0.26	protein_coding
B4GALNT3	rs1056008	12	553,672	460,364	0.85	6.71	− 1043.34	T	C	0.25	protein_coding
DDX11	rs3891006	12	31,073,506	31,073,860	0.86	− 13.25	− 1102.08	A	G	0.44	protein_coding
RPS26	rs1131017	12	56,042,145	56,041,351	0.81	− 134.34	− 929.902	C	G	0.39	protein_coding
C17orf97	rs7503725	17	410,351	410,325	0.85	1.89	− 1055.68	G	T	0.25	protein_coding
AC126544.2	rs2696531	17	46,278,268	45,586,452	0.86	1.04	− 1097.79	C	A	0.21	lincRNA
SPATA20	rs9890200	17	50,547,162	50,543,058	0.81	− 1.01	− 34.173	A	C	0.37	protein_coding
CEACAMP3	rs3745936	19	41,586,462	41,599,735	0.84	1.11	− 040.05	A	T	0.22	transcribed_unprocessed_pseudogene
PWP2	rs2277806	21	44,089,769	44,107,373	0.87	3.16	− 139.85	A	C	0.19	protein_coding
GATD3A	rs3788104	21	44,092,213	44,133,610	0.86	4.25	− 104.35	G	A	0.18	protein_coding
FAM118A	rs576259663	22	45,363,712	45,308,968	0.86	43.45	− 1108.47	T	TA	0.12	protein_coding

Table 1. Top 25 cis-eQTLs ($p < 5e{-}8$). *EA* effect allele, *OA* the other allele, *EAF* effect allele frequency; R^2 variance explained by the lead eQTL (SNP).

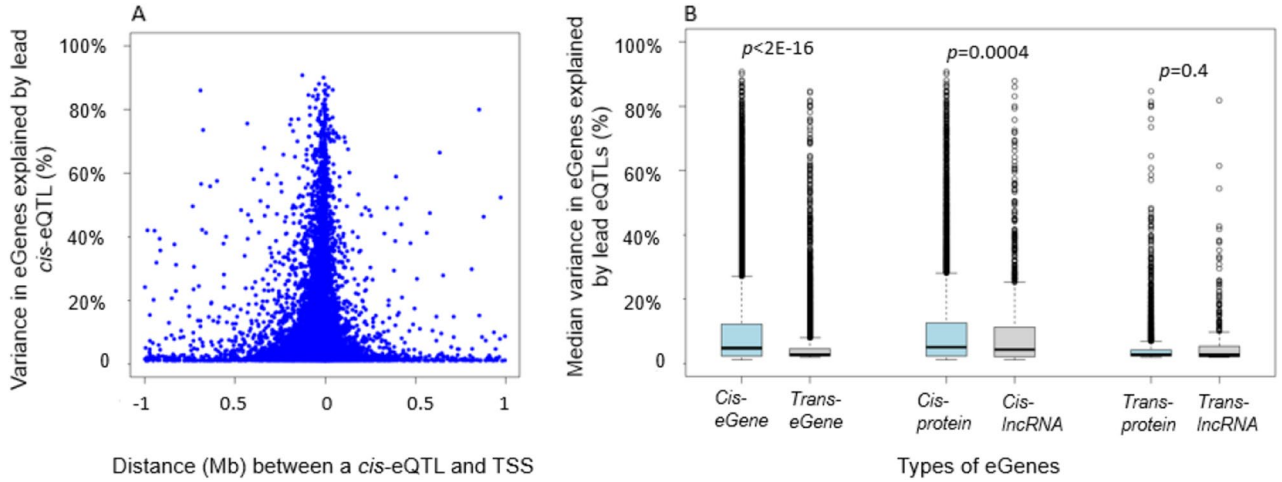

Figure 1. Variance in eGenes explained by lead e-QLT variants. (**A**) Variance in eGenes explained by lead *cis*-eQTLs in relation to the distance in mega base pairs of the lead cis-eQTLs to the transcription start site (TSS) of the *cis*-gene. (**B**) Comparison of median variance in the expression levels of eGenes explained by the lead eQTL variants. The median value of variance explained in *cis*-eGenes was significantly higher than that of *trans*-eGenes (4.8% versus 2.8%, $p < 2e{-}16$). For *cis*-eGenes, the protein-coding-eGenes had slightly higher median variance explained in the expression level than *cis*-lncRNA genes (5.1% versus 4.3%, $p = 0.0004$). No significant difference in variance explained in *trans*-eGenes of protein-coding genes versus *trans*-lncRNA genes (2.8% versus 2.7%, $p = 0.41$).

MAF range	n	Median effect size	1st Quartile effect size	3rd Quartile effect size
***Cis*-eQTL variants**				
[0.1, 0.5)	1,960,534	0.44	0.12	1.41
[0.05, 0.1)	390,362	0.64	0.17	2.02
[0.01, 0.05)	424,024	0.98	0.29	2.84
(0.003–0.01)	80,191	1.77	0.50	5.03
***Trans*-eQTL variants**				
[0.1, 0.5)	321,275	0.42	0.12	1.01
[0.05, 0.1)	81,083	0.69	0.17	1.36
[0.01, 0.05)	94,234	0.89	0.38	1.71
(0.003–0.01)	29,464	2.38	0.80	8.13

Table 2. Comparison of effect sizes of eQTLs with different minor allele frequency ranges. *MAF* minor allele frequency, *n* the number of eQTLs, *effect size* the effect size of association between eQTL and eGene.

Gene symbol	SNP	Gene Chr	SNP Chr	SNP Pos	Gene Start Pos	R^2	Beta	t value	log10P	OA	EA	EAF	Gene type
EMBP1	rs4549528	1	5	50,372,700	121,519,112	0.70	1.63	78.04	− 677.53	T	C	0.48	transcribed_unprocessed_pseudogene
AL365357.1	rs4841	1	5	150,446,963	178,411,616	0.64	2.79	67.64	− 570.81	C	T	0.25	processed_pseudogene
AL591846.1	rs13161099	1	5	150,442,799	206,695,837	0.62	1.87	65.67	− 549.988	G	A	0.25	processed_pseudogene
AC004057.1	rs1131017	4	12	56,042,145	113,214,046	0.61	− 0.42	− 63.03	− 521.823	C	G	0.39	transcribed_processed_pseudogene
RPL10P9	rs6655287	5	X	154,396,528	168,616,352	0.64	4.11	68.52	− 580.03	A	G	0.10	processed_pseudogene
PSPHP1	rs34945686	7	7	65,809,663	55,764,797	0.61	0.05	64.11	− 533.329	C	G	0.18	unprocessed_pseudogene
AC104692.2	rs6593279	7	7	55,736,277	152,366,763	0.60	0.05	62.97	− 521.195	G	A	0.20	processed_pseudogene
RNF5P1	rs8365	8	6	32,180,626	38,600,661	0.78	0.97	96.24	− 850.788	G	C	0.19	processed_pseudogene
TUBB8	rs28652789	10	16	33,807	46,892	0.61	0.32	63.35	− 525.289	G	C	0.25	protein_coding
COX20P1	rs10927332	10	1	244,837,362	68,632,371	0.62	0.10	64.57	− 538.221	C	T	0.19	processed_pseudogene
EIF2S3B	rs16997659	12	X	24,057,745	10,505,602	0.81	0.99	106.39	− 939.701	A	G	0.17	protein_coding
RPS2P5	rs2286466	12	16	1,964,282	118,246,084	0.80	71.71	101.17	− 894.683	A	G	0.21	processed_pseudogene
LINC00431	rs41288614	13	13	112,486,035	110,965,704	0.70	0.20	76.92	− 666.36	A	G	0.15	transcribed_unprocessed_pseudogene
NPIPB15	rs3927943	16	16	69,977,282	74,377,878	0.80	3.79	103.12	− 911.688	T	A	0.40	protein_coding
TUBB8P7	rs28652789	16	16	33,807	90,093,154	0.75	0.51	88.54	− 779.687	G	C	0.25	transcribed_unprocessed_pseudogene
RPL13P12	rs2280370	17	16	89,561,052	17,383,377	0.69	36.16	75.78	− 654.808	T	G	0.19	processed_pseudogene
LRRC37A2	rs56328224	17	17	45,495,053	46,511,511	0.80	5.91	101.76	− 899.821	C	T	0.24	protein_coding
POLRMTP1	rs14155	17	19	619,021	62,136,972	0.69	0.62	75.32	− 650.176	G	C	0.50	processed_pseudogene
TUBB8P12	rs2562131	18	16	33,887	47,390	0.65	0.47	68.64	− 581.244	C	A	0.25	protein_coding
AP001005.3	rs28652789	18	16	33,807	49,815	0.61	0.15	64.25	− 534.859	G	C	0.25	lincRNA
RPSAP58	rs74987185	19	3	39,414,963	23,827,162	0.84	10.17	117.60	− 1031.88	G	GCT	0.31	processed_pseudogene
GATD3B	rs2277806	21	21	44,089,769	5,079,294	0.74	− 3.83	− 84.78	− 743.85	A	C	0.19	protein_coding
FP565260.1	rs2277806	21	21	44,089,769	5,130,871	0.76	− 2.96	− 90.65	− 799.469	A	C	0.19	protein_coding
SIRPAP1	rs115287948	22	20	1,915,413	30,542,536	0.75	1.12	89.28	− 786.711	G	A	0.36	processed_pseudogene
GPX1P1	rs7643586	X	3	49,394,214	13,378,735	0.61	16.44	64.25	− 534.823	C	G	0.43	processed_pseudogene

Table 3. Top 25 top trans-eQTLs ($p < 1e{-}12$). *EA* effect allele, *OA* the other allele, *EAF* effect allele frequency, R^2 variance explained by the lead eQTL (SNP).

Variance in expression explained by lead eQTL variants. The narrow-sense heritability is the proportion of phenotypic variance explained by additive genetic effects[17]. We estimated the proportion of variance (R^2) in the expression of a gene that was explained by the lead cis-eQTL or trans-eQTL variant. We found that the median R^2 value of lead *cis*-eQTLs was significantly higher than that of lead *trans*-eQTLs (R^2 4.8% versus 2.8%, $p < 2.2e{-}16$) (Fig. 1B). For the majority of *cis*-eGenes (85%) and *trans*-eGenes (96%), the lead eQTL variants only explained a small proportion of variance in expression ($R^2 < 0.2$). The lead e-QTLs explained a large proportion of variance in expression ($R^2 > 0.8$) of an extremely small proportion of eGenes (0.17% of *cis*-eGenes and five *trans*-eGenes). We further compared the median values of *cis*-eQTL R^2 versus *trans*-eQTL R^2 between protein-coding genes and *lncRNA* genes. For *cis*-eGenes, protein-coding-eGenes had slightly higher median variance

Exposure	Chr	Gene type	Outcome	INV MR[1]			N SNPs
				Beta	SE	*p*	
PSRC1	**1**	**Protein coding**	**CHD**	**− 0.084**	**0.0075**	**4.8E−29**	**7**
LTA	**6**	**Protein coding**	**CHD**	**− 0.069**	**0.011**	**1.3E−09**	**5**
MIR6891	**6**	**miRNA**	**CHD**	**1.72**	**0.28**	**2.0E−09**	**25**
LIPA	**10**	**Protein coding**	**CHD**	**0.0033**	**0.00039**	**2.9E−17**	**18**
PHETA1	**12**	**Protein coding**	**CHD**	**− 0.078**	**0.013**	**4.7E−09**	**3**
ACSL6	5	Protein coding	COVID-19	0.19	0.064	0.0025[#]	4
DPP9	19	Protein coding	COVID-19	− 0.044	0.017	0.0078[#]	3
HLA-DRB1	6	Protein coding	COVID-19	0.00099	0.00018	1.9E−08[#]	35
IFNAR2	21	Protein coding	COVID-19	− 0.023	0.0037	1.8E−06[#]	11
OAS1	12	Protein coding	COVID-19	− 0.0086	0.0022	1.6E−04[$]	1
SLC22A31	12	Protein coding	COVID-19	0.32	0.11	0.0029	13
TYK2	21	Protein coding	COVID-19	0.011	0.0021	2.8E−08	3
AC006460.2	**2**	**Bidirectional promoter lncRNA**	**SBP**	**− 5.60**	**0.55**	**2.3E−24**	**3**
MAP4	**3**	**Protein coding**	**SBP**	**0.092**	**0.0086**	**4.6E−27**	**4**
PHETA1	**12**	**Protein coding**	**SBP**	**− 0.92**	**0.058**	**1.9E−58**	**3**
SLC5A11	**16**	**Protein coding**	**SBP**	**− 0.82**	**0.066**	**5.3E−35**	**21**
ACADVL	**17**	**Protein coding**	**SBP**	**− 0.035**	**0.0030**	**1.5E−31**	**3**

Table 4. Top results in Mendelian randomization analyses. [1]Beta/SE and p-value were obtained by inverse variance weighted MR method. [#]Heterogeneity was observed in MR analyses. Sensitivity analyses were performed with median-based and mode-based MR methods in Supplemental Table 9. [$]MR analysis was performed at gene level. At splice variation level (rs10774671), the MR $p = 4E{-}06$.

explained in their expression level than for *lncRNA* genes (5.1% versus 4.3%, $p = 0.0004$). However, we did not see this trend for *trans*-eGenes of protein-coding versus *lncRNA* genes (2.8% versus 2.7%, $p = 0.41$) (Fig. 1B).

Gene Ontology analyses. We identified 100 significant GO terms for the top 1000 *cis*-eGenes at FDR < 0.05. Of these Go terms, there were 58 for Biological Process, 31 for Cellular Component, and 11 for Molecular Function (Supplemental Table 7). Of note, the top GO terms appeared to be related to immune functions. For example, the top two Biological Processes are "leukocyte degranulation" (FDR = 1e−6) and "myeloid leukocyte mediated immunity" (FDR = 2e−6) and the top two Cellular Components are cytoplasm (FDR = 3e−6) and MHC protein complex (FDR = 6e−6). The top 1000 top *trans*-eGenes gave rise to 75 significant (FDR < 0.05) GO terms including 37 for Biological Process, 32 for Cellular Component, and 6 for Molecular Function. The top GO terms for the top 1000 *trans*-eGenes were enriched in pathways and molecular functions related to immune functions (Supplemental Table 7).

GWAS enrichment analyses. We linked 1,855,111 *cis*-eQTL variants ($P < 5e{-}8$) to GWAS Catalog variants. At FDR < 0.05, the *cis*-eQTL variants were enriched with GWAS SNPs associated with 815 traits, representing 28% of the traits in the GWAS Catalog. The top traits identified in enrichment analyses include several cardiovascular disease risk factors. For example, *cis*-eQTL variants are enriched with BMI-associated SNPs (fold enrichment = 84, FDR = 3.3e−267), total cholesterol (fold enrichment = 98, FDR = 7.3e−162) (Supplemental Table 8). We identified 193 GWAS traits enriched for the *trans*-eQTL variants (Supplemental Table 9). The top traits in the *trans* enrichment analysis included neuroticism measurement (fold enrichment = 3, FDR = 1.9e−89) and BMI-adjusted waist circumference (fold enrichment = 2, 6.4e−87).

Mendelian randomization analysis. We performed two-sample MR to test for potential causal association of the *cis*-eGenes with SBP, CAD, and COVID-19 severity. We found 1558 genes containing at least one eQTL variant (median 29; interquartile range [IQR] 6, 88) that coincided with variants from GWAS of SBP ($p < 5e{-}8$)[18]. After Bonferroni correction for multiple testing, MR identified putative causal associations for 60 genes with SBP (i.e., $p < 0.05/1558$) (Table 4, Supplemental Table 10). Of these 60 genes, six lncRNAs (AC066612.1, AC069200.1, AC092747.4, AC100810.3, AL590226.2, and LY6E-DT) showed putative causal associations with SBP. For CAD, 173 genes contained at least one eQTL variant [median 5; IQR (2, 18) that also were associated with CAD in GWAS[19]. Thirteen genes showed putative causal associations with CAD (i.e., $p < 0.05/173$) (Table 4, Supplemental Table 10); none of the 13 putative causal genes was a lncRNA. Using results of a recent GWAS of COVID-19 severity[20] and a study that investigated circulating proteins influencing COVID-19 susceptibility and severity[21], we identified 24 genes with *cis*-eQTL variants [median 3, IQR; (2, 126)] that coincide with COVID severity variants. MR analyses identified seven putatively causal genes for COVID-19 severity (Table 4, Supplemental Tables 10 and 11). Two of the genes included the 2'-5'-oligoadenylate synthetase 1 gene (*OAS1*) (MR IVW $p = 1.6E{-}04$) and the interferon-alpha/beta receptor beta chain gene (*IFNAR2*) (MR IVW $p = 1.8E{-}06$). A recent study identified an alternative splicing variant (sQTL), rs10774671, at exon 7 of *OAS1* for which the "G" allele leads to a "prenylated" protein that is protective against severe COVID[22]. Addi-

tional MR analysis using rs10774671 as the instrumental variable demonstrated that splice variation of *OAS1* is also causal for COVID-19 severity ($p = 4e{-}6$).

Replication analyses. The Battle study only provided *p* values for eQTL analyses. Of the reported 10,914 *cis*-eQTL-eGene pairs from the study by Battle et al.[23] (FDR < 0.05)[23], 6782 (62%) pairs displayed $p < 5e{-}8$ in the present study. The average proportion of variance explained by these 6782 *cis*-eQTL variants in respective genes was 0.11 (Supplemental Table 12). Of the 269 *trans*-eQTL-eGene pairs (FDR < 0.05) reported by Battle et al.[23] 47 (18%) pairs displayed $p < 1e{-}12$ in the current study. The average proportion of variance explained by these 47 *trans*-eQTL variants in respective genes was 0.076. Of note, all 47 *trans*-eQTL variants and respective *trans*-eGenes are located on the same chromosomes (Supplemental Table 13). The average distance between these *trans*-eQTL variants and respective *trans*-eGenes is within 22 Mb.

We conducted additional replication analysis for the *cis*-eQTL variant-eGene pairs generated from 8,372,247 SNPs and 20,188 gene transcripts that were common to our study (n = 2622 participants) and to GTEx(6) (n = 755 participants). At $p < 5e{-}8$, we identified 1,080,485 *cis*-eQTL variant-eGene pairs in GTEx and 3,852,182 pairs in our study; of these, 951,085 pairs (88% of pairs in GTEx) displayed the same effect direction as in our larger study. (Supplemental Fig. 3). At $p < 1e{-}4$, we identified 1,815,208 *cis*-eQTL variant-eGene pairs in GTEx and 6,364,173 pairs in this study; of these, 1,797,977 (99% of pairs in GTEx) displayed the same effect directionality with our study. As can be seen in the figure, there is considerable concordance between the Framingham Heart Study (FHS) and GTEx eQTL effect sizes, although the FHS has a larger sample size than GTEx whole blood samples (2622 vs 755), which results in a smaller standard error and larger t-statistics (Supplemental Fig. 4).

Discussion

We leveraged WGS and RNA-seq data from 2622 FHS participants to create a powerful scientific resource of eQTLs. We identified significant unique *cis*-eQTL variants-eGene pairs ($n = 2{,}855{,}111$ unique variants with *cis*-15,982 eGenes) and 526,056 unique *trans*-eQTL variants-eGene pairs (526,056 unique variants and unique 7233 *trans*-eGenes. A large proportion of reported *cis*-eQTL variant-eGene pairs were replicated with directionally concordant in our study including 88% of *cis*-variant-eGene pairs from GTEx.

Consistent with our previous study and others[7–12,24,25], 90% of eQTL variants identified in the present study are located within 1 Mb of the corresponding cis-eGene and 83% are within 100 kb of the TSSs of the corresponding eGene. While the majority of (85% of *cis*- and 96% of *trans*-) lead eQTL variants explained only a small proportion ($R^2 < 0.2$) of interindividual variation in expression of the corresponding eGenes, 15% of lead *cis*-eQTL variants and 4% of lead *trans* variant explained 20% or more of interindividual variation in expression of the corresponding eGenes[26]. Additionally, eQTL variants were enriched ($p < 0.0001$) in disease-associated SNPs identified by GWAS. We further demonstrated the utility of our eQTL resource for conducting causal inference testing. Our MR analyses revealed putatively causal relations of gene expression to several disease phenotypes including SBP, CAD, and COVID-19 severity. Taken together, the comprehensive eQTL resource we provide can advance understanding of the genetic architecture of gene expression underlying a wide variety of diseases. The interactive and browsable eQTL resource will be posted to the National Heart, Lung, and Blood Institute's BioData Catalyst site and will be freely accessible to the scientific community.

Our study expands current knowledge by creating an accessible and browsable resource of eQTLs based on WGS and RNA-seq technologies. It also includes eQTLs for lncRNAs that were not reported in prior eQTL studies that used array-based expression profiling. Over the past decade, accumulating evidence shows that lncRNAs are widely expressed and have key roles in gene regulation[27,28]. It is estimated that the human genome contains 16,000 to 100,000 lncRNAs[27]. We identified 447,598 *cis*-eQTL variants for 1518 *cis*-lncRNAs and 121,241 *trans*-eQTLs for 475 *trans*-lncRNAs (Supplemental Tables 5 and 6). In addition, we identified six lncRNAs that showed putative causal associations with SBP. However, the functions of these six lncRNAs remain to be determined. Thus, our novel eQTL database may also help in the study of non-protein-coding RNAs in relation to health and disease.

As a proof of concept of the application of the eQTL resource, we performed MR analyses on a small number of cardiovascular traits and COVID-19 severity and demonstrated that the eQTL database can identify promising candidate genes with evidence of putatively causal relations to disease that may merit functional studies. Severe acute respiratory syndrome coronavirus 2 (SARS-CoV-2) has spread across the globe and caused millions of deaths since it emerged in 2019. Recent GWAS of COVID-19 susceptibility and severity[29–31] have identified SNPs in several loci on chromosomes 3, 9 and 21[32]. Using our eQTL resource in conjunction with COVID-19 GWAS, we conducted MR analyses that identified seven genes, including *OAS1* and *IFNAR2*, as putatively causal for COVID-19 severity. The *OAS1/2/3* cluster has been identified as a risk locus for COVID-19 severity[29]. This area harbors a protective haplotype of approximately 75 kilo-bases (kb) at 12q24.13 among individuals of European ancestry[21]. A recent study identified an alternative splicing variant, rs10774671, at exon 7 of *OAS1* for which the protective allele "G" leads to a more active OAS1 enzyme[22]. Our MR results suggest that both the *OAS1* gene expression level and its splice variation are causal for COVID-19 severity.

The *IFNAR2* gene encodes a protein in the type II cytokine receptor family. Mutations in *IFNAR2* are associated with Immunodeficiency and measles virus susceptibility and play an essential and a narrow role in human antiviral immunity[33]. A recent study further showed that loss-of-function mutations in *IFNAR2* are associated with severe COVID-19[34]. These studies, considered alongside our MR results provide evidence of a causal role of *IFNAR2* expression in severe COVID-19 infection.

This study identified *cis*-eQTL in whole blood and used them as IVs in MR analyses. Therefore, caution is needed in interpreting the causal relations of several genes to several disease traits. Blood tissue is more easily accessible than other tissues, e.g., kidney or heart, for large association studies. Several previous studies of omics

data have shown that findings in whole blood were compariable to other tissues[35,36]. Several eQTL studies have also demonstrated *cis*- and *trans*-eQTLs gene regulation across tissues. The GTEx Consortium found that pervasive *cis*-eQTLs affect the majority of human genes across tissues[6,37]. Another study also showed that the identified cardiometabolic genetic loci share downstream *cis*- and *trans*-gene regulation across tissues and diseases[38].

This study has several noteworthy limitations. This study included White participants of European ancestry who were middle-aged and older; therefore, the eQTLs identified may not be generalizable to other races or age ranges. The current RNA-seq platform included ~ 7700 lncRNAs, which is a modest subset of all lncRNAs in the human genome[27]. We used MR analyses to infer causal relation of genes to disease traits. MR analysis is predicated on a set of critical assumptions that may not be testable in the setting of eQTL analysis[39,40]. Replication of our eQTL findings is warranted in studies with larger sample sizes and more diverse populations. In addition, our study found that the cis-eQTL variants were enriched for GWAS-associated SNPs. It is possible that we may have underestimated signal regions when local LD in the GWAS region was not considered. An exhaustive investigation of colocalization[41,42] is not feasible in this study due to computational burden and storage limitations.

Our study also has several strengths. The advent of high-throughput RNA sequencing technology provides an unparalleled opportunity to accelerate understanding of the genetic architecture of gene expression. Our study extends and expands the existing literature by identifying novel eQTLs based on WGS and RNA-seq. We demonstrate the potential applications of a vast eQTL resource by analyzing the concordance of eQTL variants with SNPs from GWAS of several disease phenotypes followed by causal inference analyses that identified promising disease-related genes that may merit functional studies. We created an open and freely accessible eQTL repository that can serve as a promising scientific resource to better understand of the genetic architecture of gene expression and its relations to a wide variety of diseases.

Methods

Study participants. This study included participants from the FHS Offspring[10] and Third Generation cohorts[11]. Blood samples for RNA seq were collected from Offspring participants who attended the ninth examination cycle (2011–2014) and the Third Generation participants who attended the second examination cycle (2008–2011). Protocols for participant examinations and collection of genetic materials were approved by the Institutional Review Board at Boston Medical Center. All participants provided written, informed consent for genetic studies. All research was performed in accordance with relevant guidelines/regulations.

Isolation of RNA from whole blood and RNA-seq. Peripheral whole blood samples (2.5 mL) were collected from FHS participants (Offspring participants at the ninth examination cycle and the Third Generation participants at the second examination cycle) using PAXgene™ tubes (PreAnalytiX, Hombrechtikon, Switzerland), incubated at room temperature for 4 h for RNA stabilization, and then stored at − 80 °C until use. Total RNA was isolated using a standard protocol using a PAXgene Blood RNA Kit at the FHS Genetics Laboratory (FHS Third Generation cohort) and the TOPMed contract laboratory at Northwest Genomics Center (Offspring cohort). Tubes were allowed to thaw for 16 h at room temperature. White blood cell pellets were collected after centrifugation and washing. Cell pellets were lysed in guanidinium-containing buffer. The extracted RNA was tested for its quality by determining absorbance readings at 260 and 280 nm using a NanoDrop ND-1000 UV spectrophotometer. The Agilent Bioanalyzer 2100 microfluidic electrophoresis (Nano Assay and the Caliper LabChip system) was used to determine the integrity of total RNA.

All RNA samples were sequenced by an NHLBI TOPMed program[13] reference laboratory (Northwest Genomics Center) following the TOPMed RNA-seq protocol. All RNS-seq data were processed by University of Washington. The raw reads (in FASTQ files) were aligned using the GRCh38 reference build to generate BAM files. RNA-SeQC[43] was used for processing of RNA-seq data by the TOPMed RNA-seq pipeline to derive standard quality control metrics from aligned reads. Gene-level expression quantification was provided as read counts and transcripts per million (TPM). GENCODE 30 annotation was used for annotating gene-level expression.

Whole blood cell counts. Whole blood cell counts include white blood cell (WBC) count, red blood cell count, platelet count, and WBC differential percentages (neutrophil percent, lymphocyte percent, monocyte percent, eosinophil percent, and basophil percent). Contemporaneously measured blood cell counts were available in 2094 (80%) of the 2622 FHS participants used in eQTL analyses. We performed partial least squares (PLS) prediction method[44] with three-fold cross-validation (2/3 samples for training and 1/3 for validation) to impute these blood cell components using gene expression from RNA-seq. Prediction accuracy (R-squared) varied across blood component: WBC: 0.58, platelet: 27%, neutrophil percentage: 82%, lymphocyte percentage: 85%, monocyte percentage: 77%, eosinophil percentage: 87%, basophil percentage: 32%. Because 80% of the participants in this study had directly measured cell count variables and only 20% received imputed variables, we used the measured (in 2094 participants) and predicted (in 528 participants) blood cell components as covariates in regression models for eQTL analyses.

RNA-seq quality control, and data adjustment. To minimize confounding, expression residuals were generated by regressing transcript expression level on age, sex, measured or predicted blood cell count and differential cell proportions, and genetic principal components. Principal component (PC) analysis is a technique for reducing the dimensionality in large data sets[45]. It has been widely used in regression analyses to minimize unknown confounding. We included five PCs computed from FHS genotype profiles to account for population stratification. We also included 15 PCs computed from the transcriptome profile to account for unknown confounders that may affect gene expression. In addition, we adjusted for a relatedness matrix, and technical

covariates including year of blood collection, batch (sequencing machine and time, plate and well), and RNA concentration.

Whole genome sequencing. Whole genome sequencing of genomic DNA from whole blood was conducted in ~ 6000 FHS participants as part of NHLBI's TOPMed program[13]. Standard procedures were used to obtain DNA fragmentation and library construction. Sequencing was performed by a TOPMed reference laboratory (the Broad Institute of MIT and Harvard) using Hi Seq X with sequencing software HiSeq Control Software (HCS) version 3.3.76, then analyzed using RTA2 (Real Time Analysis). The DNA sequence reads were aligned to a human genome build GRCH38 using a common pipeline across all TOPMed WGS centers. A sample's sequence was considered complete when the mean coverage of nDNA was ≥ 30x. This analysis used genetic variants generated from TOPMed Freeze 10a[13].

Association analyses of expression levels with SNPs. We performed association analyses of expression levels with genome-wide SNPs with minor allele count (MAC) ≥ 10. In a simple regression model, a SNP was used as an independent variable and the residuals of a transcript expression level was used as the dependent variable. All analyses were performed on the NIH-supported STRIDES cloud infrastructure. A graphical Processing Unit (GPU)-based program[12] was used to facilitate computation. Effect sizes, standard error, partial R-squared, and p-values for all SNP-gene expression pairs with $p < 1e{-}4$ were stored to enable lookups and to facilitate later meta-analysis. We evaluated the genomic inflation factor for eQTL analyses. Due to storage burden, we evaluated the genomic inflation factor based on full eQTL analysis (i.e., no p value restriction) on chromosome 12 because the length of this chromosome is close to the median length of chromosome 1–22.

In this study, we defined *cis*-eQTLs as targeting genes within 1 Mb of their transcription start site (TSS). *Trans*-eQTLs referred to those that were beyond of 1 Mb of the TSSs of the eGenes on the same chromosome or those on the different chromosomes of the eGenes. A significant *cis*-eQTL of an eGene was identified if a SNP within 1 Mb of that gene was associated with expression of a transcript of that gene at $P < 5 \times 10^{-8}$. A significant *trans*-eQTL was defined as a SNP beyond 1 Mb that gave rise to $P < 1 \times 10^{-12}$ in association a gene.

Estimation of variance in expression level explained by eQTLs. An accurate estimation of heritability may help understand the degree to which genetic factors influence a trait[49]. Narrow-sense heritability measures the proportion of phenotypic variance explained by additive genetic effects[17]. We estimated the proportion of variance (R^2) in the expression level of a gene that was explained by the lead *cis*-eQTL (*cis*-R^2) or trans-eQTL (*trans*-R^2) variant. We conducted Mood's median test (median_test in the "coin" R package) to compare the median value of variance in *cis*-eGenes and *trans*-eGenes explained by *cis*-eQTLs versus trans-eQTLs. For *cis*- or *trans*-eGenes, we compared the median value of genetic variance in protein-coding eGenes versus *lncRNA* eGenes.

Comparison of effect sizes of eQTLs with different minor allele frequencies. Previous studies showed that rare variants showed a large effect size in QTL analysis. For significant cis-eQTLs ($P < 5 \times 10^{-8}$) and trans-eQTLs ($P < 1 \times 10^{-12}$), we compared the median (25% quartile, 75% quartile) of the absolute values of effect sizes for eQTL variants in four intervals based on their minor allele frequencies (MAFs): [0.1, 0.5), [0.05, 0.1), [0.01, 0.05), and (0.003–0.01).

Gene Ontology analyses. We selected the single, most significant eQTL variant (i.e. lead variant) for each eGene (for the gene level analysis) from *cis*- and *trans*-eQTL results separately. The eGenes annotated to the selected lead *cis* and *trans* eQTL variants were matched into Entrez IDs. We used the "goana" function from the "limma" package[46] to test for over-representation of gene ontology (GO) terms or KEGG pathways applied to the top 1000 eGenes. We used FDR < 0.05 to report GO terms including Biological Process, Cellular Component, and Molecular Function.

Enrichment analyses using GWAS Catalog. We linked the eQTL variants with SNPs from the GWAS Catalog[2] (data downloaded on October 22, 2021), which included 243,618 entries for 2960 mapped traits at p < 5e−8. *Cis*- and *trans*-eQTL variants were analyzed separately. Unique SNP RS IDs were used for enrichment analysis with Fisher's test. FDR < 0.05 was used for significance.

Correlation analysis of selected lncRNA and protein coding genes. For lncRNAs that were in the top 25 *cis*-eQTL variant-eGene pairs, we performed partial Pearson correlation analyses between the expression level of the lncRNA and its nearby protein coding gene, adjusting for the same set of covariates that were included in eQTL analysis. We performed random sampling of 1000 genes 500 times to derive null distributions of partial Pearson correlation of these gene pairs. We calculated an empirical p-value to evaluate whether the partial Pearson correlation coefficient between the expression level of an lncRNA and its nearby protein coding gene was significantly higher than the average partial Pearson correlation coefficient from randomly selected gene pairs. The empirical p-value was calculated as the proportion of partial Pearson correlation coefficients that were more extreme than the correlation coefficient of an lncRNA and its nearby protein coding gene.

Mendelian randomization analysis. We conducted Mendelian randomization (MR) to demonstrate the application of the eQTL resource in causal inference analysis. We tested for potential causal association of the *cis*-eGenes with SBP, coronary artery disease (CAD), and COVID-19 severity. SBP-associated SNPs were obtained

from GWAS of over 1 million people[18]. CAD-associated SNPs were obtained from the study of 34,541 CAD cases and 261,984 controls of UK Biobank resource followed by replication in 88,192 cases and 162,544 controls from CARDIoGRAMplusC4D[19]. COVID-19 associated SNPs were obtained from a recent GWAS including 14,134 COVID-19 cases and 1,284,876 controls of European ancestry by the COVID-19 Host Genetics Initiative[29]. We performed two-sample MR analyses[40] using the TwoSampleMR R package[47]. The instrumental variables (IVs) were independent *cis*-eQTL variants (LD $r^2 < 0.1$) from this study. The primary analysis used the inverse variance weighted (IVW) method. We also assessed heterogeneity of the IVs in each gene and conducted sensitivity analysis using the MR-Egger method to test for potential horizontal pleiotropy. We also performed the median-based method[48] and mode-based method[49] when heterogeneity was present in MR analyses due to outliers among the IVs[50]. We reported putative causal genes if Bonferroni correction $p < 0.05/n$ (n is the number of genes tested).

Replication analyses. A previous study reported 10,914 *cis*-eQTL variant-eGene pairs and 269 *trans* pairs (FDR < 0.05) through RNA-sequencing of 922 individuals[23]. We performed replication analyses using the reported *cis- and trans*-eQTL variant-eGene pairs in conjunction with the pairs in the present study[23]. We also used the *cis*-eQTL database generated from GTEx whole blood (version 8) (https://www.gtexportal.org/home/datasets) for replication of our *cis*-QTL findings. Whole genome sequencing and RNA-seq were conducted in whole blood of 755 samples in GTEx. The replication was only performed using the *cis*-eQTL-variant-eGene pairs generated by 8,372,247 SNPs and 20,188 gene transcripts that were found in common between our study and GTEx. Because this study was aimed to provide eQTL resource for the broad scientific community, we present replication results using both $p < 5e{-}8$ and $p < 1e{-}4$ for replicating *cis*-eQTL variant-eGene pairs.

Data availability

The datasets analyzed in the present study are available at the dbGAP repository phs000007.v32.p13. The datasets analyzed in the present study are available at the dbGAP repository phs000007.v32.p13 (https://www.ncbi.nlm.nih.gov/projects/gap/cgi-bin/study.cgi?study_id=phs000007.v30.p11).

Received: 26 April 2022; Accepted: 17 November 2022
Published online: 23 November 2022

References

1. Visscher, P. M. *et al.* 10 Years of GWAS discovery: Biology, function, and translation. *Am. J. Hum. Genet.* **101**, 5–22. https://doi.org/10.1016/j.ajhg.2017.06.005 (2017).
2. MacArthur, J. *et al.* The new NHGRI-EBI Catalog of published genome-wide association studies (GWAS Catalog). *Nucleic Acids Res.* **45**, D896–D901. https://doi.org/10.1093/nar/gkw1133 (2017).
3. Consortium, E. P. An integrated encyclopedia of DNA elements in the human genome. *Nature* **489**, 57–74. https://doi.org/10.1038/nature11247 (2012).
4. Eicher, J. D. *et al.* GRASP v2.0: An update on the Genome-Wide Repository of Associations between SNPs and phenotypes. *Nucleic Acids Res.* **43**, D799-804. https://doi.org/10.1093/nar/gku1202 (2015).
5. Boyle, E. A., Li, Y. I. & Pritchard, J. K. An expanded view of complex traits: From polygenic to omnigenic. *Cell* **169**, 1177–1186. https://doi.org/10.1016/j.cell.2017.05.038 (2017).
6. The GTEx Consortium. The GTEx Consortium atlas of genetic regulatory effects across human tissues. *Science* **369**, 1318–1330. https://doi.org/10.1126/science.aaz1776 (2020).
7. Fehrmann, R. S. *et al.* Trans-eQTLs reveal that independent genetic variants associated with a complex phenotype converge on intermediate genes, with a major role for the HLA. *PLoS Genet.* **7**, e1002197. https://doi.org/10.1371/journal.pgen.1002197 (2011).
8. Westra, H. J. *et al.* Systematic identification of trans eQTLs as putative drivers of known disease associations. *Nat. Genet.* **45**, 1238–1243. https://doi.org/10.1038/ng.2756 (2013).
9. Liang, L. *et al.* A cross-platform analysis of 14,177 expression quantitative trait loci derived from lymphoblastoid cell lines. *Genome Res.* **23**, 716–726. https://doi.org/10.1101/gr.142521.112 (2013).
10. Battle, A. & Montgomery, S. B. Determining causality and consequence of expression quantitative trait loci. *Hum. Genet.* **133**, 727–735. https://doi.org/10.1007/s00439-014-1446-0 (2014).
11. Kirsten, H. *et al.* Dissecting the genetics of the human transcriptome identifies novel trait-related trans-eQTLs and corroborates the regulatory relevance of non-protein coding locidagger. *Hum. Mol. Genet.* **24**, 4746–4763. https://doi.org/10.1093/hmg/ddv194 (2015).
12. Joehanes, R. *et al.* Integrated genome-wide analysis of expression quantitative trait loci aids interpretation of genomic association studies. *Genome Biol.* **18**, 16. https://doi.org/10.1186/s13059-016-1142-6 (2017).
13. Taliun, D. *et al.* Sequencing of 53,831 diverse genomes from the NHLBI TOPMed Program. *Nature* **590**, 290–299. https://doi.org/10.1038/s41586-021-03205-y (2021).
14. Miretti, M. M. *et al.* A high-resolution linkage-disequilibrium map of the human major histocompatibility complex and first generation of tag single-nucleotide polymorphisms. *Am. J. Hum. Genet.* **76**, 634–646. https://doi.org/10.1086/429393 (2005).
15. Yao, C. *et al.* Genome-wide mapping of plasma protein QTLs identifies putatively causal genes and pathways for cardiovascular disease. *Nat Commun* **9**, 3268. https://doi.org/10.1038/s41467-018-05512-x (2018).
16. Wright, M. W. A short guide to long non-coding RNA gene nomenclature. *Hum. Genom.* **8**, 7. https://doi.org/10.1186/1479-7364-8-7 (2014).
17. Visscher, P. M., Hill, W. G. & Wray, N. R. Heritability in the genomics era–concepts and misconceptions. *Nat. Rev. Genet.* **9**, 255–266. https://doi.org/10.1038/nrg2322 (2008).
18. Evangelou, E. *et al.* Genetic analysis of over 1 million people identifies 535 new loci associated with blood pressure traits. *Nat. Genet.* **50**, 1412–1425. https://doi.org/10.1038/s41588-018-0205-x (2018).
19. van der Harst, P. & Verweij, N. Identification of 64 novel genetic loci provides an expanded view on the genetic architecture of coronary artery disease. *Circ. Res.* **122**, 433–443. https://doi.org/10.1161/CIRCRESAHA.117.312086 (2018).
20. Kousathanas, A. *et al.* Whole genome sequencing reveals host factors underlying critical Covid-19. *Nature* https://doi.org/10.1038/s41586-022-04576-6 (2022).
21. Zhou, S. *et al.* A Neanderthal OAS1 isoform protects individuals of European ancestry against COVID-19 susceptibility and severity. *Nat. Med.* **27**, 659–667. https://doi.org/10.1038/s41591-021-01281-1 (2021).

22. Bonnevie-Nielsen, V. *et al.* Variation in antiviral 2',5'-oligoadenylate synthetase (2'5'AS) enzyme activity is controlled by a single-nucleotide polymorphism at a splice-acceptor site in the OAS1 gene. *Am. J. Hum. Genet.* **76**, 623–633. https://doi.org/10.1086/429391 (2005).
23. Battle, A. *et al.* Characterizing the genetic basis of transcriptome diversity through RNA-sequencing of 922 individuals. *Genome Res.* **24**, 14–24. https://doi.org/10.1101/gr.155192.113 (2014).
24. Morley, M. *et al.* Genetic analysis of genome-wide variation in human gene expression. *Nature* **430**, 743–747. https://doi.org/10.1038/nature02797 (2004).
25. Li, Q. *et al.* Expression QTL-based analyses reveal candidate causal genes and loci across five tumor types. *Hum. Mol. Genet.* **23**, 5294–5302. https://doi.org/10.1093/hmg/ddu228 (2014).
26. Huan, T. *et al.* A systematic heritability analysis of the human whole blood transcriptome. *Hum. Genet.* **134**, 343–358. https://doi.org/10.1007/s00439-014-1524-3 (2015).
27. Statello, L., Guo, C. J., Chen, L. L. & Huarte, M. Gene regulation by long non-coding RNAs and its biological functions. *Nat. Rev. Mol. Cell Biol.* **22**, 96–118. https://doi.org/10.1038/s41580-020-00315-9 (2021).
28. He, R. Z., Luo, D. X. & Mo, Y. Y. Emerging roles of lncRNAs in the post-transcriptional regulation in cancer. *Genes Dis.* **6**, 6–15. https://doi.org/10.1016/j.gendis.2019.01.003 (2019).
29. Initiative, C.-H.G. The COVID-19 Host Genetics Initiative, a global initiative to elucidate the role of host genetic factors in susceptibility and severity of the SARS-CoV-2 virus pandemic. *Eur. J. Hum. Genet.* **28**, 715–718. https://doi.org/10.1038/s41431-020-0636-6 (2020).
30. Ellinghaus, D. *et al.* The Severe Covid-19 GWAS Group. Genomewide association study of severe Covid-19 with respiratory failure. *N. Engl. J. Med.* **383**, 1522–1534. https://doi.org/10.1056/NEJMoa2020283 (2020).
31. Li, Y. *et al.* Genome-wide association study of COVID-19 severity among the Chinese population. *Cell Discov.* **7**, 76. https://doi.org/10.1038/s41421-021-00318-6 (2021).
32. Kotsev, S. V. *et al.* Hypotheses and facts for genetic factors related to severe COVID-19. *World J. Virol.* **10**, 137–155. https://doi.org/10.5501/wjv.v10.i4.137 (2021).
33. Duncan, C. J. *et al.* Human IFNAR2 deficiency: Lessons for antiviral immunity. *Sci. Transl. Med.* **7**, 307ra154. https://doi.org/10.1126/scitranslmed.aac4227 (2015).
34. Smieszek, S. P., Polymeropoulos, V. M., Xiao, C., Polymeropoulos, C. M. & Polymeropoulos, M. H. Loss-of-function mutations in IFNAR2 in COVID-19 severe infection susceptibility. *J. Glob. Antimicrob. Resist.* **26**, 239–240. https://doi.org/10.1016/j.jgar.2021.06.005 (2021).
35. Hillman, S. L. *et al.* Novel DNA methylation profiles associated with key gene regulation and transcription pathways in blood and placenta of growth-restricted neonates. *Epigenetics* **10**, 50–61. https://doi.org/10.4161/15592294.2014.989741 (2015).
36. Yang, S. Y. *et al.* Blood-derived mitochondrial DNA copy number is associated with gene expression across multiple tissues and is predictive for incident neurodegenerative disease. *Genome Res.* **31**, 349–358. https://doi.org/10.1101/gr.269381.120 (2021).
37. Consortium, G *et al.* Genetic effects on gene expression across human tissues. *Nature* **550**, 204–213. https://doi.org/10.1038/nature24277 (2017).
38. Franzen, O. *et al.* Cardiometabolic risk loci share downstream cis- and trans-gene regulation across tissues and diseases. *Science* **353**, 827–830. https://doi.org/10.1126/science.aad6970 (2016).
39. Davies, N. M., Holmes, M. V. & Davey Smith, G. Reading Mendelian randomisation studies: A guide, glossary, and checklist for clinicians. *BMJ* **362**, k601. https://doi.org/10.1136/bmj.k601 (2018).
40. Hartwig, F. P., Davies, N. M., Hemani, G. & Davey Smith, G. Two-sample Mendelian randomization: Avoiding the downsides of a powerful, widely applicable but potentially fallible technique. *Int. J. Epidemiol.* **45**, 1717–1726. https://doi.org/10.1093/ije/dyx028 (2016).
41. Giambartolomei, C. *et al.* Bayesian test for colocalisation between pairs of genetic association studies using summary statistics. *PLoS Genet.* **10**, e1004383. https://doi.org/10.1371/journal.pgen.1004383 (2014).
42. Wallace, C. Eliciting priors and relaxing the single causal variant assumption in colocalisation analyses. *PLoS Genet.* **16**, e1008720. https://doi.org/10.1371/journal.pgen.1008720 (2020).
43. DeLuca, D. S. *et al.* RNA-SeQC: RNA-seq metrics for quality control and process optimization. *Bioinformatics* **28**, 1530–1532. https://doi.org/10.1093/bioinformatics/bts196 (2012).
44. Nguyen, D. V. Partial least squares dimension reduction for microarray gene expression data with a censored response. *Math. Biosci.* **193**, 119–137. https://doi.org/10.1016/j.mbs.2004.10.007 (2005).
45. Jolliffe, I. T. & Cadima, J. Principal component analysis: A review and recent developments. *Philos. Trans. A* **374**, 20150202. https://doi.org/10.1098/rsta.2015.0202 (2016).
46. Ritchie, M. E. *et al.* limma powers differential expression analyses for RNA-sequencing and microarray studies. *Nucleic Acids Res.* **43**, e47. https://doi.org/10.1093/nar/gkv007 (2015).
47. Hemani, G. *et al.* The MR-Base platform supports systematic causal inference across the human phenome. *Elife* https://doi.org/10.7554/eLife.34408 (2018).
48. Bowden, J., Davey Smith, G., Haycock, P. C. & Burgess, S. Consistent estimation in Mendelian randomization with some invalid instruments using a weighted median estimator. *Genet. Epidemiol.* **40**, 304–314. https://doi.org/10.1002/gepi.21965 (2016).
49. Hartwig, F. P., Davey Smith, G. & Bowden, J. Robust inference in summary data Mendelian randomization via the zero modal pleiotropy assumption. *Int. J. Epidemiol.* **46**, 1985–1998. https://doi.org/10.1093/ije/dyx102 (2017).
50. Burgess, S. *et al.* Guidelines for performing Mendelian randomization investigations. *Wellcome Open Res.* **4**, 186. https://doi.org/10.12688/wellcomeopenres.15555.2 (2019).

Disclaimer

The views and opinions expressed in this manuscript are those of the authors and do not necessarily represent the views of the National Heart, Lung, and Blood Institute, the National Institutes of Health, or the U.S. Department of Health and Human Services.

Author contributions

C.L. wrote the main manuscript text; R.J., C.L., X.S., and P.J.M. performed statistics analyses and prepared the tables and figures; Y.W., G.M.P., and A.N.P. cleaned RNAseq data; N.L.H-C., and A.N.P. coordinate data acquisition; D.L., R.J., J.M., A.K., M.S., T.H., S-J.H., H.B., B.T., P.J.M., and R.S.V. reviewed/edited the manuscript; D.C.,M.F., and N.S. performed data sharing; R.S.V. and D.L. provided funding for whole genome sequencing and RNAseq.

Funding

The Framingham Heart Study was supported by NIH contracts N01-HC-25195, HHSN268201500001I, and 75N92019D00031. DNA methylation assays were supported in part by the Division of Intramural Research

(D. Levy, Principal Investigator) and an NIH Director's Challenge Award (D. Levy, Principal Investigator). The analytical component of this project was funded by the NHLBI Division of Intramural Research (D. Levy, Principal Investigator). Whole genome sequencing for the TransOmics in Precision Medicine (TOPMed) program was supported by the NHLBI. Core support including centralized genomic read mapping and genotype calling, along with variant quality metrics and filtering were provided by the TOPMed Informatics Research Center (3R01HL-117626-02S1; contract HHSN268201800002I). Core support including phenotype harmonization, data management, sample identity QC, and general program coordination were provided by the TOPMed Data Coordinating Center (R01HL-120393; U01HL-120393; contract HHSN268201800001I). J. Ma is supported by NIH grants, K22HL135075 and R01AA028263.

Competing interests
The authors declare no competing interests.

Additional information
Supplementary Information The online version contains supplementary material available at https://doi.org/10.1038/s41598-022-24611-w.

Correspondence and requests for materials should be addressed to C.L., R.J. or D.L.

Reprints and permissions information is available at www.nature.com/reprints.

Publisher's note Springer Nature remains neutral with regard to jurisdictional claims in published maps and institutional affiliations.